ADVANCED MATERIALS
www.advmat.de

Reverse Saturable Absorption Induced by Phonon-Assisted Anti-Stokes Processes

*Xiangling Tian, Rongfei Wei, Qianyi Guo, Yu-Jun Zhao, and Jianrong Qiu**

In materials showing reverse saturable absorption (RSA), optical transmittance decreases at intense laser irradiation. One approach to application of these materials is to protect the sensors or human eyes from laser damage. To date, research has mainly concentrated on thin films and suspensions of graphite and its nanostructure (including nanotubes, graphene, and graphene oxides), which are mainly used as an optical limiter for nanosecond laser pulses. Moreover, thin individual pieces of semiconductor usually exhibit increased transmittance due to saturable absorption when the laser energy (E_{laser}) is higher than the band gap (E_B). Here, it is shown that indirect gap semiconductor WSe_2 exhibits high RSA on exposure to a femtosecond laser under $E_{laser} > E_B$ near band gap excitation, which is attributed to the longitudinal optical phonon-assisted anti-Stokes transition by the annihilation of phonons and the absorption of photons. An optical limiting threshold (≈21.6 mJ cm^{-2}) lower than those reported for other optical-limiting materials currently for femtosecond laser at 800 nm is observed.

The ability to manipulate the shape and intensity of laser pulses employing nonlinear optical (NLO) materials opens new horizons and huge opportunities to practical application in a number of advanced optical technologies.[1–4] The NLO process (saturable absorption, SA; reverse saturable absorption, RSA or optical limiting, OL) is closely connected with the Stokes or anti-Stokes process, especially for NLO materials based on semiconductors. Carriers (electrons) in semiconductor materials are excited from the valence band into the conduction band through absorbing one or more photons, and then scattered to an internal state via the creation or annihilation of phonons following the relationship,[5] $\omega_{internal} = \omega_{photon} \pm n\omega_{phonon}$ (ω is a frequency and n is an integer), which corresponds to the Stokes or anti-Stokes process, just as shown in **Scheme 1**. When the initial empty states are occupied by the excited carriers (electrons), the absorption become saturated (Scheme 1a for SA), which can be used to account for the mechanism of most of saturable absorbers based on semiconductors.[1,6,7] Excited states absorption (ESA, Scheme 1b) usually happens in molecular system to absorb two photons to create a highly excited carrier by using intermediate real electronic states, which is similar to free carrier absorption (FCA) in semiconductor.[8,9] Except Cr^{4+}:GSGG saturable absorber[10] using ESA to account for SA behavior to generate a passively Q-switched laser, ESA is widely used to illustrate the mechanism of RSA.[11–13] Two-photon absorption (TPA, Scheme 1c) uses a virtual intermediate state to absorb two photons to excite a high energy carrier,[9] which contributes to a large RSA response and breaks the limitation of excitation source. Alternatively, the anti-Stokes energy transfer (ET, Scheme 1d) is an energy shift via a real intermediate state to generate a higher energy carrier,[4,8] which is usually involved in heterostructures to account for RSA response.[4,14] Phonon-assisted (PA) anti-Stokes (Scheme 1e) is usually used to realize light-induced cooling in polar semiconductors such as GaAs,[15] GaInP/GaAs,[16] and ZnTe[5] by the annihilation of one or multiple phonons. Up to now, the RSA behavior of semiconductor induced by the PA anti-Stokes has only reported in a small amount of semiconductors when the energy of pump laser (E_{laser}) is lower than the band gap (E_B) ($E_{laser} < E_B$).[8,17] However, despite PA optical absorption transition has been theoretically proved in indirect semiconductor when $E_{laser} > E_B$,[18–20] it is difficult to achieve RSA induced by PA anti-Stokes when $E_{laser} > E_B$ in transition-metal dichalcogenides (TMDCs) system due to the weak excited carrier (exciton)–phonon coupling, especially in indirect gap TMDCs semiconductor.

Phonons, which are quanta of lattice vibrations, can intervene in the carrier transition through deformation potential interaction (acoustic phonons) or Fröhlich interaction (optical/homopolar phonons).[21–27] Because of the high exciton binding energies in TMDCs system, the deformation coupling related with acoustic phonons is likely to occur with less

Dr. X. Tian, Dr. Q. Guo, Prof. J. Qiu
State Key Laboratory of Luminescent Materials and Devices
School of Materials Science and Engineering
South China University of Technology
Wushan Road 381, Guangzhou 510641, P. R. China
E-mail: qjr@zju.edu.cn
Dr. R. Wei
Department of Physics
Zhejiang Normal University
Jinhua, Zhejiang 321004, P. R. China
Prof. Y.-J. Zhao
Department of Physics
South China University of Technology
Guangzhou 510640, China
Prof. J. Qiu
State Key Laboratory of Modern Optical Instrumentation
College of Materials Science and Engineering
Zhejiang University
Hangzhou, Zhejiang 310027, P. R. China

DOI: 10.1002/adma.201801638

© 2018 WILEY-VCH Verlag GmbH & Co. KGaA, Weinheim

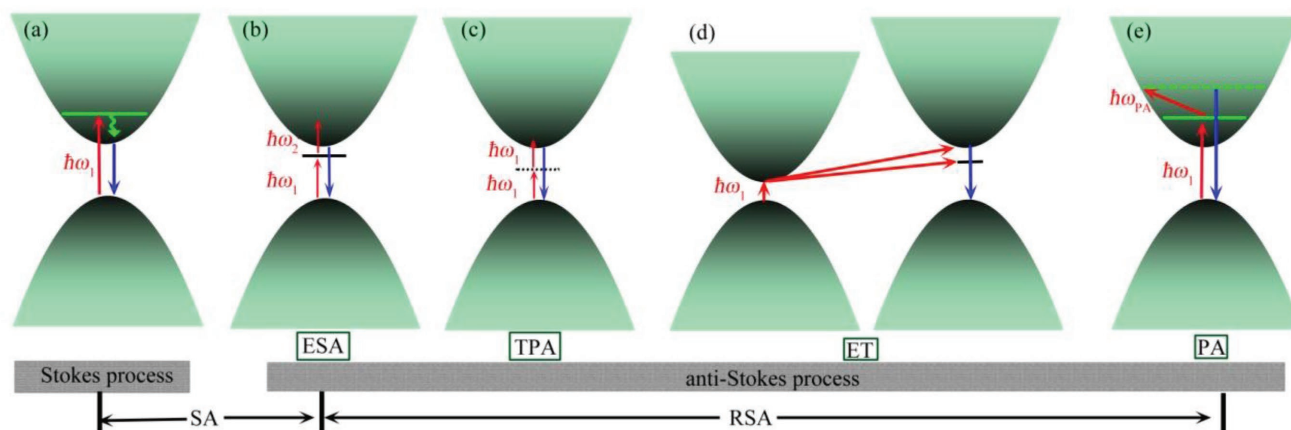

Scheme 1. Electron transition schematics. a) Saturable absorption (SA) induced by Stokes transition (low-conversion). Reverse saturable absorption (RSA) mainly induced by anti-Stokes transition includes: b) excited states absorption (ESA)-induced upconversion process via a real electronic state to absorb two photons. c) Two-photon absorption (TPA)-induced upconversion through virtual electronic state to absorb two photons. d) Energy-transfer (ET)-induced upconversion via a real intermediate state to excite a higher energy carrier. e) Phonon-assisted (PA) anti-Stokes through the absorption of photons and phonons to generate a higher energy carrier.

efficiency.[23,28,29] When excited by a resonant laser near the band gap edge of zinc telluride nanorods, the enhancement in the scattering cross of longitudinal optical (LO) phonon is much higher than that of the transverse optical (TO) modes, leading a dominant Fröhlich electron (exciton)–LO phonon interaction.[25] A large laser cooling by 40 K can be obtained under the strong coupling through upconversion process accompanied with the resonant annihilation of multiple LO phonons.[22] More importantly, the Fröhlich interaction in TMDCs systems is confirmed to be much higher than assumed in previous ab initio studies,[24] which are promising to realize RSA through the absorption of photons and the annihilation of phonons, i.e., PA anti-Stokes. According to the report by Xiong and co-workers,[22,30] the PA anti-Stokes induced emission exhibits a largest shift in CdS with the thickness of about 70 nm; that is, the exciton–phonon coupling is the strongest under the thickness of ≈70 nm. Although the monolayer TMDCs have high efficiency photoluminescence (PL) due to the direct gap semiconductor,[31,32] the PL in indirect gap one is rather too weak[33] to record many details about the carriers (electrons) transition when the thickness increases. In recent years, Z-scan technique with femtosecond (fs) pulse is a rapid and sensitive method to characterize carrier transition in the correlated materials through recording NLO response.[4,13,34–36] The intensity of fs pulse can reach up to be ≈1 GW cm^{-2},[4,13,34] which can cause the PA anti-Stokes process in TMDCs systems. These signify that the PA anti-Stokes process in multilayer TMDCs under $E_{laser} > E_B$ can be observed by choosing an appropriate technique.

In this work, we employed chemical vapor deposition (CVD) technique to synthesize high quality WSe_2 crystals with the uniformity thickness of about 60 nm to enhance the coupling between the exciton and the phonon. Detailed CVD method can be found in the Supporting Information. In order to avoid TPA in TMDCs system, the energy of the pump laser is a little bit higher than the band gap.[37] According to the calculations and PL spectrum, the band gap of multilayer WSe_2 (E_B) is near 1.44 eV. We used the fs laser with the energy of 1.55 eV (800 nm) to facilitate carriers (electrons) from the valence band to the conduction band, what usually happens is SA response under the condition. Z-scan NLO measurements display the RSA response, which is attributed to the excited carriers (electrons) transition into higher excited states by the annihilation of LO phonons and the absorption of three photons. The demonstration of RSA induced by PA anti-Stokes in multilayer WSe_2 (indirect semiconductor) exhibits unconventional implications to NLO, particularly important for pushing OL threshold to lower values (≈21.6 mJ cm^{-2}). Furthermore, these excellent NLO properties also afford the demonstration of indirect semiconductor as simple and effective components for photoelectric applications.

Figure 1a shows a typical optical image of the as-grown WSe_2. The most investigations of WSe_2 relied on mechanically exfoliated samples for now;[33,38,39] however, the size of the exfoliated WSe_2 is too small with lack of uniformity to be used to investigate NLO properties, particularly to detect PA anti-Stokes transition. By contrast, a uniform thickness WSe_2 with the controllable layer can be obtained using CVD method.[6,32] Atomic force microscopy (Figure 1b) image reveals that the thickness of the crystal is ≈57.8 nm, corresponding to ≈82 sandwiched Se–W–Se layers.[40] Similar to graphite, bulk WSe_2 possess a laminated structure with monolayer stacking, where the individual layer is bonded to another via weak van der Waals interactions,[38,39,41] as shown in **Figure 2**b,c. Arora et al.[42] recently reported that the strength of excitonic binding as well as the character of excitonic state varies from non-Rydberg states in monolayer to rather like Rydberg states in bulk, indicating the enhancement in coupling of exciton and phonon for multilayer WSe_2 compared to the monolayer. Two photoluminescence (PL) peaks located at ≈1.41 and ≈1.49 eV are exhibited in Figure 1c, where the former is related to the indirect band gap (Γ to Γ-K) and the latter is according to the direct band gap transition (K to K),[33,39,43] respectively. Since multilayer WSe_2 is an indirect band gap semiconductor, phonon absorption or release should be required for carrier transition between the valence band and the conduction band to change carriers' momentum.[23,44] For

© 2018 WILEY-VCH Verlag GmbH & Co. KGaA, Weinheim

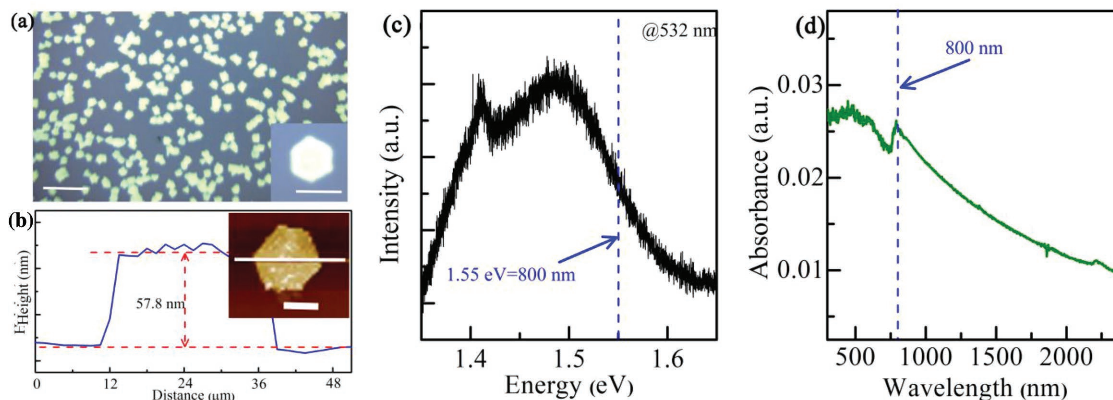

Figure 1. a) Optical image of WSe_2 crystal and the inset is enlarged image. Scale bar are 200 and 20 µm, respectively. b) Atomic force microscopy (AFM) height showing the thickness of the crystal is about 57.8 nm. The inset is image of the crystal on SiO_2/Si substrate. Scale bar: 10 µm. c) PL spectrum excited by a laser with 532 nm at room temperature. PL spectra excited by an 800 nm laser can be found in the Supporting Information. d) Optical absorption of WSe_2 crystal.

precisely this reason, PL signal is expected to be rather weak in intensity for multilayer WSe_2 as compared to that for monolayer or bilayer.[33] The main PL peak shifts to 1.46 eV when the excitation wavelength is 800 nm, as depicted in Figure S3b of the Supporting Information. The prepared WSe_2 contains a band gap of ≈1.44 eV with strong hybridization between d states of "W" and s states of "Se" around Fermi energy, as shown in Figure 2d,e, which is differentiable from the bulk sample with a band gap of ≈1.11 eV (Figure 2a). As one of layered TMDCs, monolayer WSe_2 has large electron–hole binding energies E_b of ≈0.5 eV at low temperature;[45] that is to say, the lowest energy representing optical transition is about 0.5 eV below the electronic band gap E_B. Since the Coulomb interaction decreases due to the increased dielectric screening, the binding energy greatly reduces for multilayer WSe_2.[33,45,46] At room temperature, the binding energy also greatly reduces due to the thermal effect, compared with the case at low temperature.[28,39,43,45,46] PL spectroscopy is a direct and powerful technique to identify the band gap in semiconductor systems.[42,47] As such, there is a tiny distinction between the PL measurement value and the calculation value. Figure 1d shows the ultraviolet–visible–near infrared absorption spectrum of multilayer WSe_2 on the quartz substrate, exhibiting a main absorption near the band gap.[48] The absorption spectrum was acquired using a spectrophotometer versus an uncoated quartz substrate as reference. The wavelength of fs laser (800 nm) just locates at the main absorption region, i.e., the incoming electromagnetic wave is resonance with the energy of the exciton states.[37,45] The exciton–phonon coupling can be enhanced when the irradiation laser is in resonance with excitons, and the enhancement increases with an increasing number of layers,[49] which is consistent with our design. The characteristic Raman peak intensity at around 250 cm^{-1} excited by 785 nm (near the band gap edge) enhances about tens of times than that at the excitation wavelength of 532 nm, as shown in Figure S3 of the Supporting Information, suggesting the occurrence of the resonance enhancement effect.[22,48,50] To clearly display the resonance effect, PL spectra were conducted under different irradiation powers at the excitation wavelengths of 800 nm (Figure S3b, Supporting Information), presenting the similar enhancement pattern when compared to that excited by a 532 nm laser. The linear dependence on excitation power of the luminescence confirms the one-photon related PL,[51] showing the irradiation energy of 800 nm is higher than the gap, i.e., $E_{laser} > E_B$. Compared to

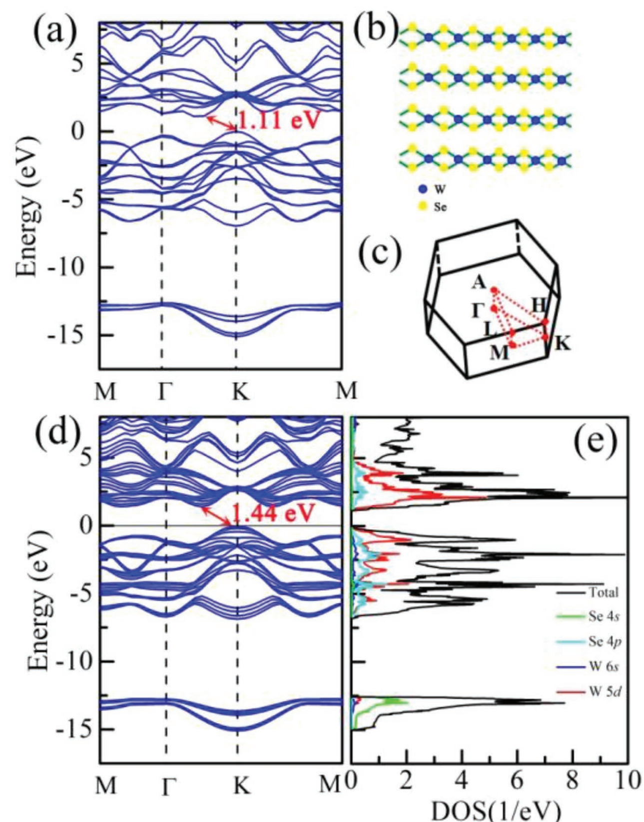

Figure 2. a) Electronic band structure calculated from first-principles density functional theory (DFT) for bulk-WSe_2. An indirect band gap of ≈1.11 eV is shown, which occurs at K and K-Γ. b) Side view of multilayer WSe_2. c) Brillouin zone of WSe_2. d) Electronic band structure and e) corresponding total and partial density of states of multilayer WSe_2. An indirect band gap of ≈1.44 eV is shown. The total density of state (DOS) is divided by 4 and the Fermi level is set to 0 eV.

© 2018 WILEY-VCH Verlag GmbH & Co. KGaA, Weinheim

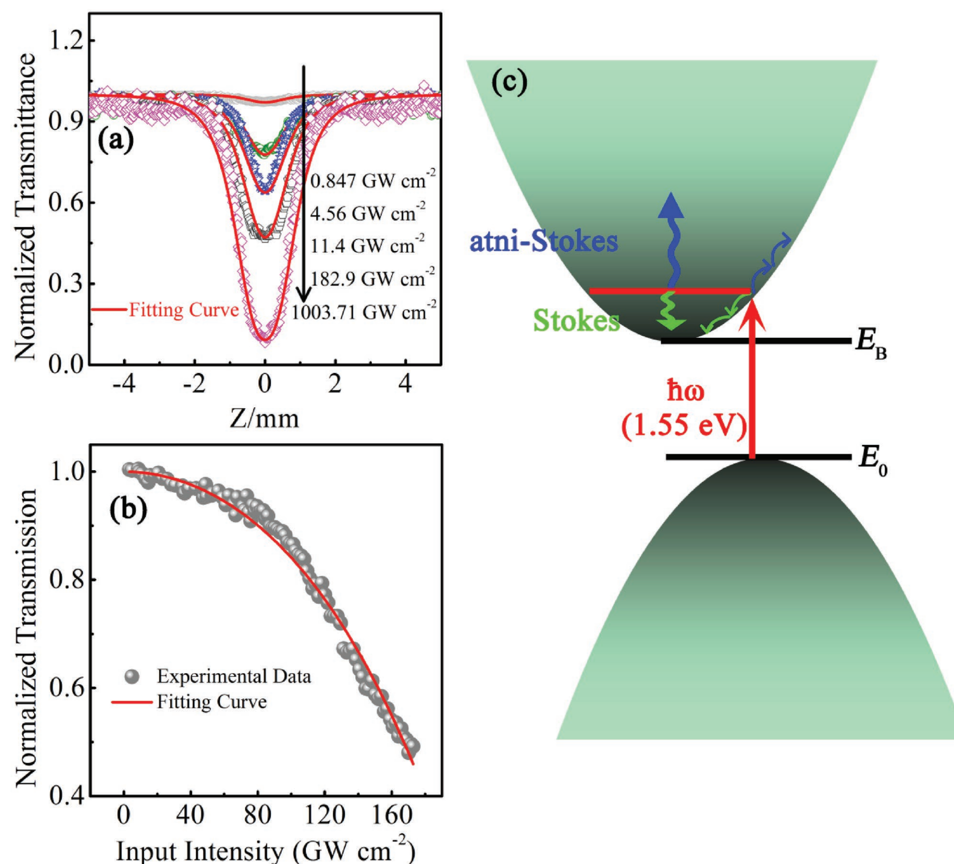

Figure 3. a) Open-aperture (OA) Z-scans of the WSe_2/quartz substrate under the excitation of 800 nm with different pulse intensities (from ≈0.847 to ≈1003.7 GW cm^{-2}). b) Three-photon absorption-induced nonlinear transmission as a function of the input intensity. The red line is the best fits given by the three-photon absorption model in the Supporting Information. c) RSA response process of the multilayer WSe_2 crystals.

direct semiconductors, the cutoff wavelength (λ_{cutoff}) is fuzzy, indicating that in addition to the intrinsic absorption of the semiconductor, there exist other absorption styles, such as impurity absorption, lattice resonance absorption and FCA, which usually occurs in the long wavelength region ($\lambda > \lambda_{cutoff}$, where $\lambda_{cutoff} = 1240/E_B$ nm).[41,45,52,53] Here, the operating wavelength of 800 nm ($\lambda_{laser} < \lambda_{cutoff}$, or $E_{laser} > E_B$) we employed can avoid the influence of these factors above. Raman spectrum, XPS, and TEM are also investigated to characterize the as-grown WSe_2 (in the Supporting Information).

Next we explore the nonlinear characteristics of the as-grown WSe_2 crystals using Z-scan measurements with the fs pulse at 800 nm under a range of input intensities from ≈0.847 to ≈1003.71 GW cm^{-2}. More details can be found in the Supporting Information as well as our previous work.[4,13,54] Shown in **Figure 3**a, all the transmittance exhibit a decrease at the position close to the focus, suggesting the occurrence of RSA response; that is, the total transmittance decreases as the intensity of the irradiation beam increases (the WSe_2 moves from nonfocus to on-focus, Z→0). In other words, the multilayer WSe_2 can suppress high intensity beam but allow high pass for low intensity light. For TMDCs[7,13,37] or black phosphorus (BPs),[55] they usually present SA response when the $E_{laser} > E_B$; however, the pronounced RSA are observed for the prepared multilayer WSe_2. Several mechanisms are generally accepted to explain the RSA, including TPA or multiphoton absorption (MPA), ESA, FCA, nonlinear scattering, and thermal lensing.[9,13,56] Since the TPA/MPA only occurs when $E_{laser} < E_B$ through the simultaneous absorption of two or more photons via virtual states, TPA/MPA cannot be used to explain the RSA of the as-grown WSe_2 due to $E_{laser} > E_B$.[56] For the case of $E_{laser} > E_B$, SA behavior can be obtained; on increasing the incident intensity, ESA induced by higher intensity can translate the SA into RSA behavior.[13,57] Only RSA behavior is recorded when the irradiation intensity increases over three orders of magnitude range from ≈0.847 to ≈1003.71 GW cm^{-2}. ESA in semiconductor materials with quasi-continuous levels is one kind of sequential single-photon absorption process in the absorption of excited state is larger than that of the ground state[9,13,57,58] According to Zhang et al.,[8] the character can be confirmed using the relationship curve of Z-scan normalized transmittance change (ΔT) and the excitation power. As shown in Figure S5a of the Supporting Information, the slop (slop ≈0.34 for three photons absorption) derived from a linear fit (log–log scale) is three-photon absorption behavior,[8] suggesting ESA not the cause of RSA in multilayer WSe_2 under $E_{laser} > E_B$. Additionally, an RSA behavior was found for BPs nanosheets dispersed in NMP as the laser intensity increased under $E_{laser} > E_B$, which is caused by bubbles around BPs induced by thermal effect under high power irradiation.[59] The WSe_2 on the quartz for measuring has no

© 2018 WILEY-VCH Verlag GmbH & Co. KGaA, Weinheim

organic-solvent around, which decides nonlinear scattering or thermal lensing caused by microplasma and microlens to be not the cause of RSA.[56,60] FCA is ineffective against causing RSA characteristic of WSe_2 under the $\lambda_{laser} < \lambda_{cutoff}$, due to its intrinsic intraband transition located in the long wave region outside the intrinsic limit (i.e., $\lambda_{laser} > \lambda_{cutoff}$), and semiconductor impurity absorption have the same reason not causing RSA response.[9,53] Therefore, new mechanism must be deliberated based on the results and discussions above.

As the multilayer WSe_2 moves from nonfocus to on-focus, the intensity of the incident beam varies from the low intensity to the high intensity, corresponding to Stokes and anti-Stokes in the WSe_2, respectively. For the low intensity case, electrons are pumped from the valence band to the conduction band and subsequently occupy the empty energy states.[13] The excited electrons can simultaneously return to the valence band, accompanying with Stokes emission. Due to the low concentration of the excited carriers and free photons in the conduction band (low intensity of the irradiation beam), the multilayer WSe_2 does not experience the NLO response (SA or RSA response). By contrast, when the WSe_2 suffers from the irradiation of the high intensity ($Z \rightarrow 0$), on the one hand, the concentration of the excited carriers (electrons) increases drastically, as well as free photons; on the other hand, it enhances the resonance coupling between the excited carriers and the phonons when the TMDCs with the thickness of ≈60 nm are subjected by an 800 nm fs laser near the band gap edge.[16,18–20,22,49,61] In semiconductors, FCA is also assisted by phonons; that is, when $\lambda_{laser} > \lambda_{cutoff}$, electrons (holes) can be promoted into higher (lower) states by absorbing addition photons in the conduction (valence) band, which is assisted by phonons during the process.[9,17] For TMDCs, the formation of exciton occurs at the noncentral points in the momentum space, which is different from the conventional semiconductors (such as GaAs) mainly at the center of the Brillouin zone center.[23,62] The electrons jump into the conduction band with a nonzero wavevector when TMDCs are excited by the irradiation energies higher than the band gap. The exciton electrons can relax to the zero wavevector state through emitting LO phonons (acoustic phonons with less efficiency),[23] which is Stokes process (corresponding SA or PL emission). Furthermore, under strong coupling between electrons and LO phonons when the irradiation resonances with the exciton near the band gap, the electrons with higher energies can be obtained via upconversion process accompanied with the resonant annihilation of multiple LO phonons;[22] that is, the excited electrons (or excitons) jump into higher states by the absorption of photons and the annihilation of phonons, which corresponds anti-Stokes process (RSA), as depicted in Figure 3c. Benefitting from the PA anti-Stokes transition, SA response never happened under the condition of $E_{laser} > E_B$. This process is similar to the report by Xiong and co-workers about laser cooling of CdS by the resonant annihilation of multiple phonons in upconversion process, stimulating carriers located at low excited state to transfer into higher excited state.[22] The higher excited state means the more empty state for carriers to achieve RSA.[4,9,13] The transition from the low excited states to high excited states in the conduction band, not only increases the energy of the excited carriers, but also changes the momentum, especially in indirect semiconductor.[8,33] The transition is on ultrafast time scale,[63,64] and the excellent NLO performance is induced by PA-anti Stokes process, which has great potential in practical applications.

The normalized transmission as a function of input laser intensity is shown in Figure 3b, and the data can be well fitted using three-photon model in the Supporting Information. The extracted unsaturated three-photon absorption coefficient (γ_0) is about -3.05 cm^3 GW^{-2} (without saturable in Figure 3b). Figure S5b of the Supporting Information shows reciprocal transmission versus irradiance in a wider range. The dashed line is the theoretical variation for a constant γ, whereas the red solid line is the theoretical variation of γ on increasing the irradiation power. From the fit, we obtain $\gamma_0 = -7.36$ cm^3 GW^{-2} and I_{sat} = 865.31 GW cm^{-2} for high irradiation power. The change of γ_0 stimulates us to explore the three-photon absorption coefficient (γ) with varying irradiance. The coefficient γ can be extracted from the fitting curves in Figure 3a using Equation (S9) in the Supporting Information, presenting a monotonic variability (shown in **Figure 4**a) which is attributed to a giant exciton effect and the resonance effect near the band edge.[26,27,45,48–50] Another critical parameter to evaluate the NLO property, OL threshold (F_{OL}), which is defined as incident fluence while the normalized transmittance decreasing to 50%,[65] can be extracted from Figure 4b. The OL threshold is about 21.6 mJ cm^{-2} under fs pulse at 800 nm, with the threshold lower than those of previously reported for other OL materials,

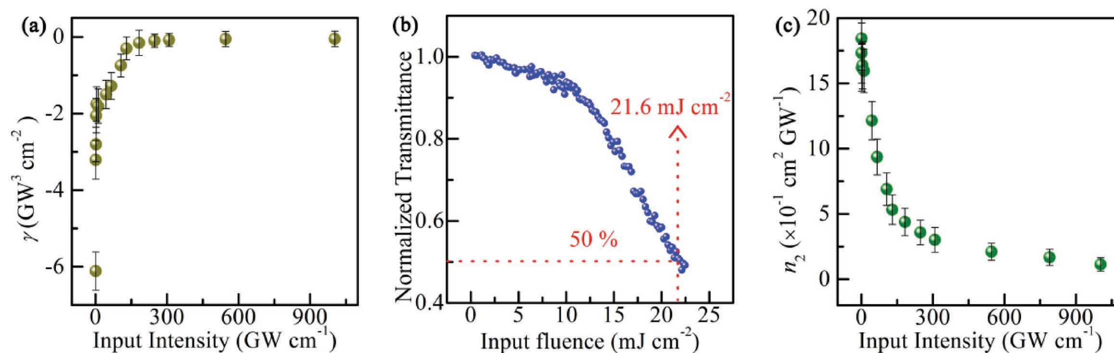

Figure 4. a) Corresponding three-photon absorption coefficient as a function of the input intensity. b) The normalized transmission as a function of input fluencies. c) Dependence of n_2 on the input intensity for multilayer WSe_2.

© 2018 WILEY-VCH Verlag GmbH & Co. KGaA, Weinheim

for example conjugated organic molecules (≈117 mJ cm^{-2}),[66] metal nanoparticles (≈26 000 mJ cm^{-2}),[67] carbon nanodots (≈74 mJ cm^{-2}),[65] graphene oxide (≈37 mJ cm^{-2}), and MoS_2 nanosheets (≈44 mJ cm^{-2}),[65,66] indicating the WSe_2 has a great potential practical application in fs lasing safety, such as the protection of eyes and sensor focal-plane arrays. Furthermore, typical closed-aperture (CA) Z-scan curves and its dividing curves by OA Z-scan (CA/OA) were also investigated. Figure S6 of the Supporting Information shows the classifications under the irradiation of ≈11.4, ≈182.9, and ≈1003.71 GW cm^{-2}, respectively. The extracted nonlinear refraction n_2 under different irradiances are summarized in Figure 4c, showing a monotonic decreasing behavior which may be attributed to the exciton effect as well as the resonance effect near the band edge.[26,27,45,48–50] Such large n_2 and low F_{OL} indicate a giant promising application as advanced optoelectronic device, particularly as optical limiter for fs laser. The demonstration of PA anti-Stokes induced RSA also suggests indirect semiconductor promising photoelectric applications without worrying low PL efficiency.

In summary, the reverse saturable absorption induced by phonon assisted anti-Stokes in multilayer WSe_2 under $E_{laser} > E_B$, has been investigated by Z-scan technique with femtosecond laser pulses. Uniformity thickness of WSe_2 is controlled as about 60 nm via chemical vapor deposition technique to enhance the coupling of excited carriers (excitons) and phonons. Carriers are resonantly injected by femtosecond laser with the wavelength of 800 nm. The observed reverse saturable absorption is attributed to the transition of the excited carrier into a higher state by the annihilation of phonons and the absorption of photons in the conduction band. Furthermore, we observed optical limiting threshold (≈21.6 mJ cm^{-2}) lower than those reported for other optical limiting materials currently for femtosecond laser pulse at 800 nm, making the indirect semiconductor WSe_2 promising as advanced nonlinear optoelectronic components, especially for femtosecond lasing safety. The demonstration of RSA induced by PA anti-Stokes exhibits unconventional implications to NLO in WSe_2, particularly important for comprehensive understanding NLO, as well as for pushing indirect semiconductor for photoelectric applications.

Supporting Information

Supporting Information is available from the Wiley Online Library or from the author.

Acknowledgements

This work was financially supported by the National Key R&D Program of China (Grant No. 2018YFB1107200), the National Natural Science Foundation of China (Grant Nos. 51472091, 51772270), Guangdong Natural Science Foundation (Grant No. S2011030001349), Fundamental Research Funds for the Central Universities (Grant No. 2013ZM0001). This work was also supported by the Natural Science Foundation of Zhejiang Province (Grant No. LQ18A040004). Open Funds from the State Key Laboratory of High Field Laser Physics of Shanghai Institute of Optics and Fine Mechanics (Chinese Academy of Sciences) and State Key Laboratory of Precision Spectroscopy of East China Normal Uniersity.

Conflict of Interest

The authors declare no conflict of interest.

Keywords

anti-Stokes, chemical vapor deposition, nonlinear optical, reverse saturable absorption, WSe_2

Received: March 13, 2018
Revised: April 12, 2018
Published online: May 23, 2018

[1] U. Keller, *Nature* **2003**, *424*, 831.
[2] F. Wang, A. G. Rozhin, V. Scardaci, Z. Sun, F. Hennrich, I. H. White, W. I. Milne, A. C. Ferrari, *Nat. Nanotechnol.* **2008**, *3*, 738.
[3] G.-K. Lim, Z.-L. Chen, J. Clark, R. G. S. Goh, W.-H. Ng, H.-W. Tan, R. H. Friend, P. K. H. Ho, L.-L. Chua, *Nat. Photonics* **2011**, *5*, 554.
[4] R. Wei, X. Tian, Z. Hu, H. Zhang, T. Qiao, X. He, Q. Chen, Z. Chen, J. Qiu, *Opt. Express* **2016**, *24*, 25337.
[5] J. Zhang, Q. Zhang, X. Wang, L. C. Kwek, Q. Xiong, *Nat. Photonics* **2016**, *10*, 600.
[6] Q. Bao, H. Zhang, Y. Wang, Z. Ni, Y. Yan, Z. X. Shen, K. P. Loh, D. Y. Tang, *Adv. Funct. Mater.* **2009**, *19*, 3077.
[7] S. Wang, H. Yu, H. Zhang, A. Wang, M. Zhao, Y. Chen, L. Mei, J. Wang, *Adv. Mater.* **2014**, *26*, 3538.
[8] Q. Zhang, X. Liu, M. I. B. Utama, G. Xing, T. C. Sum, Q. Xiong, *Adv. Mater.* **2016**, *28*, 276.
[9] Y. Chen, T. Bai, N. Dong, F. Fan, S. Zhang, X. Zhuang, J. Sun, B. Zhang, X. Zhang, J. Wang, W. J. Blau, *Prog. Mater. Sci.* **2016**, *84*, 118.
[10] G. Xiao, M. Bass, *IEEE J. Quantum Elect.* **1997**, *33*, 41.
[11] W. Su, T. M. Cooper, M. C. Brant, *Chem. Mater.* **1998**, *10*, 1212.
[12] C. W. Spangler, *J. Mater. Chem.* **1999**, *9*, 2013.
[13] R. Wei, H. Zhang, X. Tian, T. Qiao, Z. Hu, Z. Chen, X. He, Y. Yu, J. Qiu, *Nanoscale* **2016**, *8*, 7704.
[14] B. Qu, Q. Ouyang, X. Yu, W. Luo, L. Qi, Y. Chen, *Phys. Chem. Chem. Phys.* **2015**, *17*, 6036.
[15] E. Finkeißen, M. Potemski, P. Wyder, L. Viña, G. Weimann, *Appl. Phys. Lett.* **1999**, *75*, 1258.
[16] B. Imangholi, M. P. Hasselbeck, M. Sheik-Bahae, R. I. Epstein, S. Kurtz, *Appl. Phys. Lett.* **2005**, *86*, 081104.
[17] L. W. Tutt, T. F. Boggess, *Prog. Quantum Electron.* **1993**, *17*, 299.
[18] S. Imhof, A. Thränhardt, *Phys. Rev. B* **2010**, *82*, 085303.
[19] W. E. Engeler, M. Garfinkel, J. J. Tiemann, *Phys. Rev. Lett.* **1966**, *16*, 239.
[20] M. Zacharias, C. E. Patrick, F. Giustino, *Phys. Rev. Lett.* **2015**, *115*, 177401.
[21] D. Kozawa, R. Kumar, A. Carvalho, K. Kumar Amara, W. Zhao, S. Wang, M. Toh, R. M. Ribeiro, A. H. Castro Neto, K. Matsuda, G. Eda, *Nat. Commun.* **2014**, *5*, 4543.
[22] J. Zhang, D. Li, R. Chen, Q. Xiong, *Nature* **2013**, *493*, 504.
[23] A. Thilagam, *J. Appl. Phys.* **2016**, *120*, 124306.
[24] T. Sohier, M. Calandra, F. Mauri, *Phys. Rev. B* **2016**, *94*, 085415.
[25] Q. Zhang, J. Zhang, M. I. B. Utama, B. Peng, M. de la Mata, J. Arbiol, Q. Xiong, *Phys. Rev. B* **2012**, *85*, 085418.
[26] K. Siantidis, V. M. Axt, T. Kuhn, *Phys. Rev. B* **2001**, *65*, 035303.
[27] I. K. Oh, J. Singh, A. Thilagam, A. S. Vengurlekar, *Phys. Rev. B* **2000**, *62*, 2045.
[28] M. M. Ugeda, A. J. Bradley, S.-F. Shi, F. H. da Jornada, Y. Zhang, D. Y. Qiu, W. Ruan, S.-K. Mo, Z. Hussain, Z.-X. Shen, F. Wang, S. G. Louie, M. F. Crommie, *Nat. Mater.* **2014**, *13*, 1091.
[29] K. F. Mak, C. Lee, J. Hone, J. Shan, T. F. Heinz, *Phys. Rev. Lett.* **2010**, *105*, 136805.

 © 2018 WILEY-VCH Verlag GmbH & Co. KGaA, Weinheim

[30] D. Li, J. Zhang, Q. Xiong, *Opt. Express* **2013**, *21*, 19302.
[31] M. Amani, D.-H. Lien, D. Kiriya, J. Xiao, A. Azcatl, J. Noh, S. R. Madhvapathy, R. Addou, S. KC, M. Dubey, K. Cho, R. M. Wallace, S.-C. Lee, J.-H. He, J. W. Ager, X. Zhang, E. Yablonovitch, A. Javey, *Science* **2015**, *350*, 1065.
[32] X. Tian, R. Wei, S. Liu, Y. Zhang, J. Qiu, *Nanoscale* **2017**, *10*, 752.
[33] H. Sahin, S. Tongay, S. Horzum, W. Fan, J. Zhou, J. Li, J. Wu, F. M. Peeters, *Phys. Rev. B* **2013**, *87*, 165409.
[34] B. S. Kalanoor, L. Gouda, R. Gottesman, S. Tirosh, E. Haltzi, A. Zaban, Y. R. Tischler, *ACS Photonics* **2016**, *3*, 361.
[35] R. Zhang, J. Fan, X. Zhang, H. Yu, H. Zhang, Y. Mai, T. Xu, J. Wang, H. J. Snaith, *ACS Photonics* **2016**, *3*, 371.
[36] S. J. Varma, J. Kumar, Y. Liu, K. Layne, J. Wu, C. Liang, Y. Nakanishi, A. Aliyan, W. Yang, P. M. Ajayan, J. Thomas, *Adv. Opt. Mater.* **2017**, *5*, 1700713.
[37] Y. Li, N. Dong, S. Zhang, X. Zhang, Y. Feng, K. Wang, L. Zhang, J. Wang, *Laser Photonics Rev.* **2015**, *9*, 427.
[38] M. Koperski, K. Nogajewski, A. Arora, V. Cherkez, P. Mallet, J. Y. Veuillen, J. Marcus, P. Kossacki, M. Potemski, *Nat. Nanotechnol.* **2015**, *10*, 503.
[39] W. Zhao, Z. Ghorannevis, L. Chu, M. Toh, C. Kloc, P.-H. Tan, G. Eda, *ACS Nano* **2013**, *7*, 791.
[40] H. Zhou, C. Wang, J. C. Shaw, R. Cheng, Y. Chen, X. Huang, Y. Liu, N. O. Weiss, Z. Lin, Y. Huang, X. Duan, *Nano Lett.* **2015**, *15*, 709.
[41] C. Poellmann, P. Steinleitner, U. Leierseder, P. Nagler, G. Plechinger, M. Porer, R. Bratschitsch, C. Schüller, T. Korn, R. Huber, *Nat. Mater.* **2015**, *14*, 889.
[42] A. Arora, M. Koperski, K. Nogajewski, J. Marcus, C. Faugeras, M. Potemski, *Nanoscale* **2015**, *7*, 10421.
[43] J. Huang, L. Yang, D. Liu, J. Chen, Q. Fu, Y. Xiong, F. Lin, B. Xiang, *Nanoscale* **2015**, *7*, 4193.
[44] B. K. Ridley, *Electrons and Phonons in Semiconductor Multilayer*, Cambridge University Press, New York **2009**.
[45] G. Wang, X. Marie, I. Gerber, T. Amand, D. Lagarde, L. Bouet, M. Vidal, A. Balocchi, B. Urbaszek, *Phys. Rev. Lett.* **2015**, *114*, 097403.
[46] H. M. Hill, A. F. Rigosi, C. Roquelet, A. Chernikov, T. C. Berkelbach, D. R. Reichman, M. S. Hybertsen, L. E. Brus, T. F. Heinz, *Nano Lett.* **2015**, *15*, 2992.
[47] A. Steinhoff, J. H. Kim, F. Jahnke, M. Rösner, D. S. Kim, C. Lee, G. H. Han, M. S. Jeong, T. O. Wehling, C. Gies, *Nano Lett.* **2015**, *15*, 6841.
[48] E. del Corro, H. Terrones, A. Elias, C. Fantini, S. Feng, M. A. Nguyen, T. E. Mallouk, M. Terrones, M. A. Pimenta, *ACS Nano* **2014**, *8*, 9629.
[49] B. R. Carvalho, L. M. Malard, J. M. Alves, C. Fantini, M. A. Pimenta, *Phys. Rev. Lett.* **2015**, *114*, 136403.
[50] S. Zhang, N. Dong, N. McEvoy, M. O'Brien, S. Winters, N. C. Berner, C. Yim, Y. Li, X. Zhang, Z. Chen, L. Zhang, G. S. Duesberg, J. Wang, *ACS Nano* **2015**, *9*, 7142.
[51] X. Wang, H. Zhou, S. Yuan, W. Zheng, Y. Jiang, X. Zhuang, H. Liu, Q. Zhang, X. Zhu, X. Wang, A. Pan, *Nano Res.* **2017**, *10*, 3385.
[52] M. Lax, E. Burstein, *Phys. Rev.* **1955**, *97*, 39.
[53] P. A. Schumann, R. P. Phillips, *Solid-State Electron.* **1967**, *10*, 943.
[54] R. Wei, H. Zhang, Z. Hu, T. Qiao, X. He, Q. Guo, X. Tian, Z. Chen, J. Qiu, *Nanotechnology* **2016**, *27*, 305203.
[55] S. B. Lu, L. L. Miao, Z. N. Guo, X. Qi, C. J. Zhao, H. Zhang, S. C. Wen, D. Y. Tang, D. Y. Fan, *Opt. Express* **2015**, *23*, 11183.
[56] J. Wang, Y. Hernandez, M. Lotya, J. N. Coleman, W. J. Blau, *Adv. Mater.* **2009**, *21*, 2430.
[57] Z. Liu, Y. Wang, X. Zhang, Y. Xu, Y. Chen, J. Tian, *Appl. Phys. Lett.* **2009**, *94*, 021902.
[58] Q. Li, C. Liu, Z. Liu, Q. Gong, *Opt. Express* **2005**, *13*, 1833.
[59] J. Huang, N. Dong, S. Zhang, Z. Sun, W. Zhang, J. Wang, *ACS Photonics* **2017**, *4*, 3063.
[60] K. Wang, Y. Feng, C. Chang, J. Zhan, C. Wang, Q. Zhao, J. N. Coleman, L. Zhang, W. J. Blau, J. Wang, *Nanoscale* **2014**, *6*, 10530.
[61] N. Kumar, Q. Cui, F. Ceballos, D. He, Y. Wang, H. Zhao, *Phys. Rev. B* **2014**, *89*, 125427.
[62] A. M. Jones, H. Yu, N. J. Ghimire, S. Wu, G. Aivazian, J. S. Ross, B. Zhao, J. Yan, D. G. Mandrus, D. Xiao, W. Yao, X. Xu, *Nat. Nanotechnol.* **2013**, *8*, 634.
[63] K.-G. Zhou, H.-L. Zhang, *Small* **2015**, *11*, 3206.
[64] K.-G. Zhou, M. Zhao, M.-J. Chang, Q. Wang, X.-Z. Wu, Y. Song, H.-L. Zhang, *Small* **2015**, *11*, 694.
[65] R. Wei, H. Zhang, X. He, Z. Hu, X. Tian, Q. Xiao, Z. Chen, J. Qiu, *Opt. Mater. Express* **2015**, *5*, 1807.
[66] R. Wei, X. Tian, H. Zhang, Z. Hu, X. He, Z. Chen, Q. Chen, J. Qiu, *J. Alloys Compd.* **2016**, *684*, 224.
[67] L. Polavarapu, N. Venkatram, W. Ji, Q.-H. Xu, *ACS Appl. Mater. Interfaces* **2009**, *1*, 2298.

 © 2018 WILEY-VCH Verlag GmbH & Co. KGaA, Weinheim